ACS APPLIED MATERIALS & INTERFACES

Research Article

www.acsami.org

Guided Transport of Water Droplets on Superhydrophobic–Hydrophilic Patterned Si Nanowires

Jungmok Seo, Soonil Lee, Jaehong Lee, and Taeyoon Lee*

Nanobio Device Laboratory, School of Electrical and Electronic Engineering, Yonsei University, 134 Shinchon-Dong, Seodaemun-Gu, Seoul 120-749, Republic of Korea

Supporting Information

ABSTRACT: We present a facile method to fabricate hydrophilic patterns in superhydrophobic Si nanowire (NW) arrays for guiding water droplets. The superhydrophobic Si NW arrays were obtained by simple dip-coating of dodecyltrichlorosilane (DTS). The water contact angles (CAs) of DTS-coated Si NW arrays drastically increased and saturated at the superhydrophobic regime (water CA $\geq$ 150°) as the lengths of NWs increased. The demonstrated superhydrophobic surfaces show an extreme water repellent property and small CA hysteresis of less than 7°, which enable the water droplets to easily roll off. The wettability of the DTS-coated Si NW arrays can be converted from superhydrophobic to hydrophilic via UV-enhanced photodecomposition of the DTS, and such wettability conversion was reproducible on the same surfaces by repeating the DTS coating and photodecomposition processes. The resulting water guiding tracks were successfully demonstrated via selective patterning of the hydrophilic region on superhydrophobic Si NW arrays, which could enable water droplets to move along defined trajectories.

KEYWORDS: *wettability conversion, silicon nanowires, aqueous electroless etching, surface modification, UV illumination, superhydrophobic–hydrophilic pattern*

1. INTRODUCTION

Superhydrophobic surfaces with extremely water repellent properties have received considerable attention as they have various applications including self-cleaning fabrics,[1,2] antifog windows,[3,4] drag reduction,[5] and droplet manipulation.[6] By definition, a surface is superhydrophobic when the surface has a water contact angle (CA) greater than 150° with a water sliding angle less than 10°, which produces a nonwetting surface. It has been theoretically and experimentally understood that superhydrophobic surfaces can be achieved by a combination of low surface energy and topographically roughened surface structures.[7,8]

In particular, patterning of extremely hydrophilic regions on superhydrophobic surfaces is crucial in practical applications such as open channel microfluidic systems,[9,10] water harvesting surfaces,[11] highly efficient biomolecule analysis,[12−14] biospecific cell adhesive surfaces,[15,16] dynamic solubility control of nanoparticles,[17] and dynamic solution transfers.[18−22] Several researchers have reported on the methods to obtain superhydrophobic surfaces featuring hydrophilic patterns, including mussel-inspired dopamine coatings using a soft-lithography technique,[23] ultraviolet (UV)-stimulated photocatalytic decomposition of the TiO_2 nanostructure,[24] garvanic displacement reactions,[25] and the use of photopatternable polymer mixture of UV curable epoxy resin (SU-8) and polytetrafluoroethylene (PTFE) nanoparticles.[10] Superhydrophobic surfaces with hydrophilic patterns can also be fabricated via conventional photo lithography and plasma treatments.[13,14,26−28] Although the aforementioned techniques are efficient ways to obtain superhydrophobic surfaces with hydrophilic patterns, these methods require additional complex processes and are not suited for many practical applications where the control of the direction of water droplet displacement is necessary, in integration with Si-based electronics.

Here, we demonstrate a facile method to create redefinable hydrophilic patterns on superhydrophobic Si nanowire (NW) arrays as a fluidic guiding track. Superhydrophobic Si NW arrays with extreme water repellent properties were achieved by a simple dip-coating process in a dodecyltrichlorosilane (DTS) solution. The fabricated superhydrophobic Si NW arrays exhibited very low CA hysteresis and extremely low sliding angles, confirming that the resulting surface follows the Cassie state model. The hydrophilic pattern of water guiding tracks were defined on the superhydrophobic Si NW arrays by a UV-enhanced selective patterning process. The phenomenon of UV-enhanced chemical decomposition of the organic layer on the Si NW arrays was investigated using X-ray photoelectron spectroscopy (XPS) analyses and CA measurements. Changes of surface wettability from superhydrophobic to hydrophilic may be attributed to the photodecomposition of DTS alkyl chains on superhydrophobic Si NW arrays, thereby locally altering the surface energy. The motions of the water droplets

Received: August 31, 2011
Accepted: November 17, 2011
Published: November 17, 2011

were precisely controlled along the trajectory of the selectively patterned hydrophilic water guiding tracks, and such patterns could be redefined via the repetition of coating and decomposition of DTS.

2. EXPERIMENTAL SECTION

Vertically aligned Si NW arrays were fabricated on (100) oriented p-type Si wafer substrates (1−10 Ω cm) using an aqueous electroless etching (AEE) method described in details elsewhere.[29] The bare Si substrate was cleaned with a RCA solution (1:1:5(v/v/v) $NH_4OH/H_2O_2/H_2O$) at 70 °C for 10 min, followed by dipping into a 5% HF aqueous solution for 3 min at room temperature to remove the native oxide. The cleaned substrate was immediately dipped into 30 mM of $AgNO_3$ and 4.9 M of HF at 80 °C for various etching times (t_e). The silver dendrites and byproducts generated during NW fabrication were removed by successive rinsing of the substrate with a 30 wt % HNO_3 aqueous solution and deionized water. The removal of the oxide layer and resultant surface termination with hydrogen to hinder the formation of native oxide were performed by dipping the Si NW arrays in 5% HF for 3 min, followed by cleaning with deionized water at room temperature.

The surfaces of Si NW arrays were modified by immersing the samples in a 3 mM solution of DTS dissolved in hexane for 30 min at room temperature. The samples were cleaned with ethanol to remove residual reactants and dried by a nitrogen air stream. Then, the samples were baked at 150 °C for 1 h to obtain dense organic layer on the Si NW arrays. The same surface treatment was also performed on a flat Si substrate for reference.

The wettability of the Si NW arrays was manipulated by exposure to UV light. The DTS-coated Si NW arrays were directly exposed to a 75 W mercury lamp at a working distance of 3 cm for varying illumination times. The mercury lamp emitted UV light at 185 and 254 nm wavelengths, and the light intensity was maintained at 500 $\mu W/cm^2$. Superhydrophobic−hydrophilic patterns for guiding water droplets were defined using shadow masks under the same UV illumination conditions for 3 h.

The surface morphologies and chemical compositions of Si NW arrays were examined using a JEOL JSM-6360 field emission scanning electron microscope (FE-SEM) and a VG ESCALAB 220i-XL photoelectron spectroscopy system (VG Instruments) with an Al Kα monochromatized X-ray source, respectively. Water CAs were measured using ∼7.5 μL droplets of deionized water with a CA instrument (Phoenix 300, SEO Co., Ltd.) equipped with a dynamic image capture camera.

3. RESULTS AND DISCUSSION

Si NW arrays were fabricated using the AEE method. The formation of vertically aligned Si NW arrays can be attributed to the electrochemical reactions of Si substrate in the $AgNO_3$/HF solution; when the Si substrate is dipped into the mixture solution, Ag^+ ions near the Si surface are deposited on the Si substrate by capturing electrons from the valence band of Si. The deposited Ag nuclei attract electrons from the Si substrate and become negatively charged due to their relatively large electronegativity. The charged Ag nuclei act as catalysts that induce subsequent reductions of Ag^+ ions in the solution and corresponding oxidation of Si at the interfaces between Si and Ag nuclei. The Ag nuclei become larger as more Ag^+ ions are deposited, and the generated SiO_2 layer is subsequently etched by HF. Consequently, this sequential oxidation and etching process creates highly dense etch-pits on the surface, which results in vertically aligned Si NW arrays. The corresponding galvanic reactions at the interfaces between Ag nanoparticles and Si substrates are as follows[30]

$$\text{Anode: } Si + 6F^- \rightarrow SiF_6^{2-} + 4e^- \quad (1)$$

$$\text{Cathode: } Ag^+ + e^- \rightarrow Ag \quad (2)$$

$$\text{Overall: } Si + 6F^- + 4Ag^+ \rightarrow SiF_6^{2-} + 4Ag \quad (3)$$

Images a and b in Figure 1 show typical SEM cross-sectional and top-view images of the as-received Si NW arrays with a t_e of

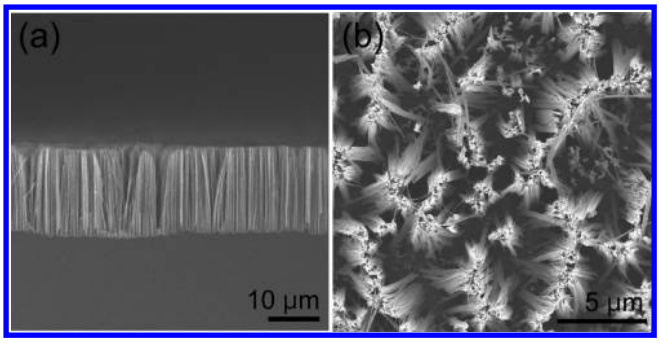

Figure 1. Typical SEM images of (a) cross-sectional and (b) top views of Si NWs fabricated using the AEE method with a t_e of 30 min.

30 min, respectively. The Si NWs were successfully formed with uniform length (∼15 μm) and vertically aligned over a large area. The measured diameters of the Si NWs in the higher magnification images (not shown) ranged from 100 to 150 nm. In addition, as shown in the top-view SEM image, the Si NWs were bundled at their tips, which can be attributed to the capillary forces of the liquid during the drying process of the substrate. The lengths, diameters of the fabricated Si NWs and the density of the bundled tips were almost identical in all the samples of Si NWs fabricated under the same conditions.

To identify the structural effects of the DTS-coated Si NW arrays on surface wettability, dynamic water CAs were measured by varying the length of the Si NWs. The lengths of the Si NWs were simply adjusted by varying t_e; the length increased proportionally with increasing t_e, where the measured length (on average) of the Si NWs increased from 0.2 to 14.7 μm as t_e varied from 2 to 30 min. Figure 2a plots the advancing and receding CAs of water droplets on the surfaces of DTS-coated Si NW arrays as a function of t_e. The water CAs of the DTS-coated Si NWs were measured at five different locations and then averaged. The uncertainties of water CAs shown in Figure 2a were very small (≤7°), which indicates that the DTS molecules were uniformly coated on the surfaces of the Si NW arrays. The advancing and receding CAs of the water droplets on the flat Si substrates with DTS layers were 109.3 and 92.6°, respectively. The CAs increased as the etching process was performed. A drastic increase of the CAs was observed at t_e between 0 to 3 min, followed by a moderate increase and saturation of the CAs ≥ 150°, of which the corresponding t_e was greater than 10 min. In addition, when the water CAs were greater than 150°, the CA hysteresis (advancing CA − receding CA) was less than 10° and the water droplets on DTS-coated Si NW arrays easily rolled off with a very low tilt angle (less than 5°). A similar relationship between the lengths of the hydroxyl alkyl-coated Si NWs and the corresponding water CAs was observed in previous research.[31,32] Figure 2b shows photographs of the dynamic motions of water droplets at rest (left) and moving (right) on DTS-coated samples when t_e was 30 min. The water droplets on Si NW arrays tended to move even when the surface was horizontal (with no intentional tilt angle),

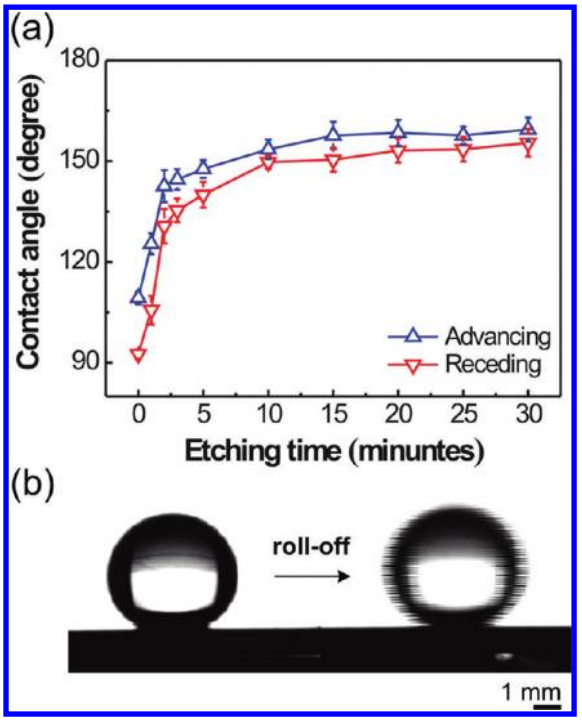

Figure 2. (a) Advancing and receding water CAs of surface modified Si NW arrays as a function of t_e. (b) Water droplet on a surface-modified Si NW array (left). The water droplet easily rolled off in the absence of any tilt angle, and the droplet edge is blurred because of the fast movement of the water droplet (right).

which clearly shows the extreme water repellent characteristics of the fabricated DTS-coated Si NW arrays.

The resulting superhydrophobic surfaces with extreme water repellent properties and Si NW length-dependent wettability could be explained by the Cassie state model.[33] According to this model, the water CA can be directly influenced by the fraction of solid−liquid contact area (f_1) and fraction of the solid-trapped air contact area (f_2), which is related to the following equation

$$\cos\theta_c = f_1 \cos\theta - f_2, \quad (4)$$

where θ_c is the measured CA on a rough surface and θ is the intrinsic CA on a flat surface. In our model system, the parameters f_1 and f_2 are affected by the lengths of the DTS-coated Si NW arrays. As shown in Figure 1b, the Si NW arrays exist as bundles, which were immediately generated at the beginning of the etching process. The formation of Si NW bundles with lowered surface energies from DTS coating created trapped air pockets between the water droplets and the top surfaces of Si NW bundles, which water could not enter, resulting in a decrease of f_1 and an increase of f_2. The increase in the lengths of the Si NWs and consequently the sizes of the Si NWs bundles with respect to t_e contributed to the increase of water CAs by further decreasing f_1 and increasing f_2.[34,35]

Figure 3 shows the variation of the static, advancing and receding water CAs of ~15-μm long DTS-coated Si NW arrays with respect to increasing UV illumination time (t_i) under ambient conditions. The static water CAs were gradually decreased from 158° to nearly zero (<5°) with increasing t_i to 180 min, and then became saturated. This wettability conversion from superhydrophobic to hydrophilic can be attributed to the decomposition of the DTS alkyl chains

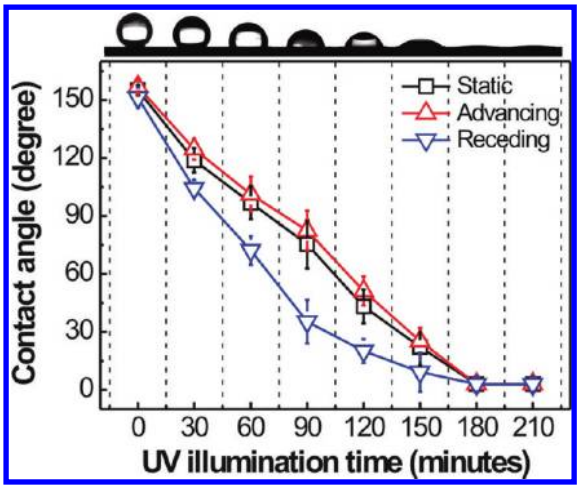

Figure 3. Optical photographs of a water droplet on DTS modified Si NW arrays as t_i increased (above) and changes of the static, advancing, and receding water CAs as a function of t_i (below). Square, triangle, and inverted triangle symbols represent the static CAs, advancing CAs, and receding CAs, respectively.

adsorbed on the Si NW arrays by UV illumination. Specifically, alkyl chains of the organic layer coated on solid surfaces were decomposed by OH radicals and atomic oxygen, catalyzed by the UV-assisted dissociation of ozone which are photo-generated in air.[36] As t_i increases, the ratio between the advancing CA and receding CA (advancing CA/receding CA) monotonically increase, as shown in Figure 3. This increase is attributed to the increased interaction between water molecules and the surfaces of Si NWs: as the DTS molecules coated on the Si NW arrays were decomposed by UV exposure, the more hydrophilic Si NW surfaces were exposed, which resulted in increased interactions between water droplets and the hydrophilic regions of the Si NWs.[37]

The UV-enhanced alkyl chain decomposition process was further examined by SEM and XPS analyses. Figure 4a−d are typical top-view SEM images of the DTS-coated Si NW arrays with varying t_i from 0 to 180 min. After the DTS coating process, the excessive DTS molecules agglomerate, leading to form carbon residues at the tips of the bundled NW arrays, as indicated by an arrow in Figure 4a. The excessive DTS were gradually decomposed via UV-enhanced photodecomposition process, and the agglomerated DTS were almost eliminated as t_i increased (Figure 4b−d). Note that the excessive DTS residues were observed only at the tips of the bundled Si NW arrays, and there were no significant morphological changes on the sides of Si NWs. The surface chemical composition of the DTS-coated Si NW arrays for various t_i were determined through XPS analyses. Figure 4e−g represents typical XPS spectra obtained from the DTS-coated Si NW arrays by varying t_i from 0 to 180 min. Figure 4e exhibits a single peak feature that is associated with the C 1s bands at binding energies between 282 and 288 eV. The peaks of C 1s are positioned at 285.1 eV, and therefore can be assigned to the C−C bond in the saturated carbon chain.[38] The peak intensity decreased as the UV illumination process proceeded, which indicates that UV illumination gradually decomposed the alkyl chains of the DTS layers on the Si NW array surfaces. Only residual carbon remained on the Si NW surfaces after the UV-enhanced decomposition process was terminated (t_i = 180 min). As shown in Figure S1, two C-related peak intensities associated

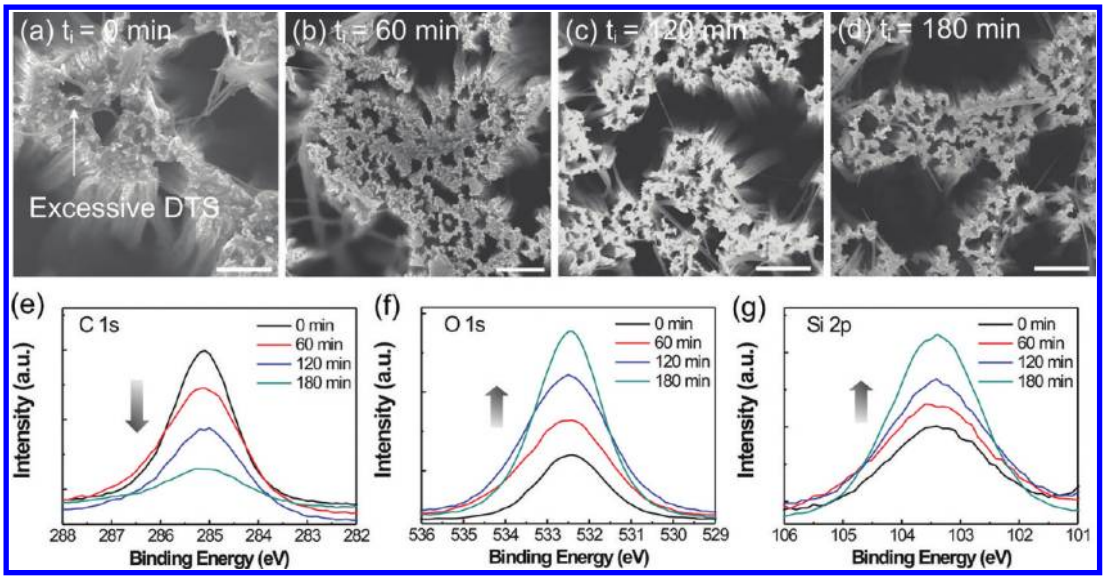

Figure 4. Typical top-view SEM images of the DTS-coated Si NW arrays at (a) t_i = 0 min, (b) t_i = 60 min, (c) t_i = 120 min, and (d) t_i = 180 min. The scale bars in the images indicate 1 μm. XPS spectra of (e) C 1s, (f) O 1s, and (g) Si 2p for the DTS-coated Si NW arrays of which t_i was varied from 0 to 180 min.

with C−O bonds (286.5 eV) and C═O bonds (289 eV) were slightly increased after the decomposition process in the high-resolution XPS spectra due to the fact that the carbon bound with hydroxyl and/or carboxyl groups as alkyl chains were decomposed during the photodecomposition process. Figure 4f, g show typical XPS spectra of O 1s and Si 2p with increasing t_i, respectively. The peaks of the XPS spectra of O 1s and Si 2p, which correspond to the Si−O bonds, are located at 532.3 and 103.1 eV, respectively.[39] Both peak intensities increased with longer t_i, as the bare Si NW surfaces became exposed due to the decompositions of DTS molecules. Furthermore, the increases in the peak intensities may be attributed to the formation of native oxide on the exposed NW surfaces. Since the DTS coating process was performed on Si NW arrays immediately after the removal of the native oxide, the hindered formation of the native oxide layer may have been proceeds on the surfaces of Si NWs, leading to the increment of peak intensities associated with Si−O bonds.[40]

The selective wettability conversion of the DTS-coated Si NW arrays was demonstrated by performing a photodecomposition process on only half of the substrate using a shadow mask. Figure 5a shows a photograph of the wettability contrast between the DTS-coated region (left) and the UV-illuminated area (right) on the same substrates of Si NW arrays. After 180 min of t_i, the wettability of the UV exposed area was fully converted from superhydrophobic to hydrophilic. Alternatively, the covered area remained superhydrophobic with extreme water repellent properties. In fact, the water CA after UV illumination is slightly increased in comparison with as-fabricated Si NWs (from 0 to <5°), which may be attributed to the remaining carbon residues, as observed in the XPS analyses on the Si NW arrays in Figure 4e. Figure 5b represents the reversible extreme wettability conversions of the Si NW arrays, indicating that the wettability conversion between superhydrophobic and hydrophilic could be successfully repeated within our experimental ranges. There were no significant changes in the water CAs of repeated cycles. The amounts of carbon residues observed in the XPS data for C 1s core level were also almost the same after repeating the coating and photodecomposition process, as shown in Figure S2 in the Supporting Information.

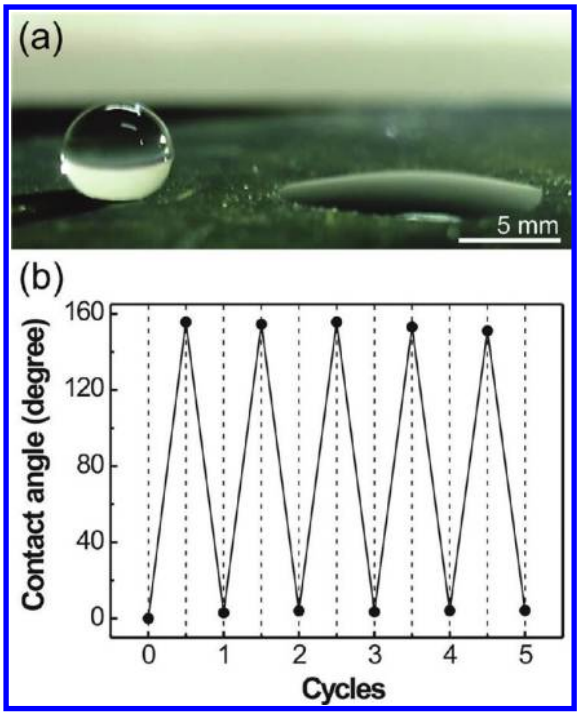

Figure 5. (a) Photograph of the wettability contrast between the DTS-coated region (left) and UV-treated region on the same substrate with Si NW arrays. (b) Reversible wettability conversion of the Si NW arrays between superhydrophobic and hydrophilic was achieved by repeating the coating and decomposition process of DTS.

To demonstrate a practical application of the selective superhydrophobic−hydrophilic patterning and reversible wettability conversion of the Si NW arrays, we created a redefinable, water guiding track with a line width of 500 μm. In the experiment, the substrates containing hydrophilic patterns were tilted with a low angle of 5°, as illustrated in Figure 6a. Figure 6b) is composed of time-sequential photographs of an 8 μL

dx.doi.org/10.1021/am2011756 | ACS Appl. Mater. Interfaces 2011, 3, 4722–4729

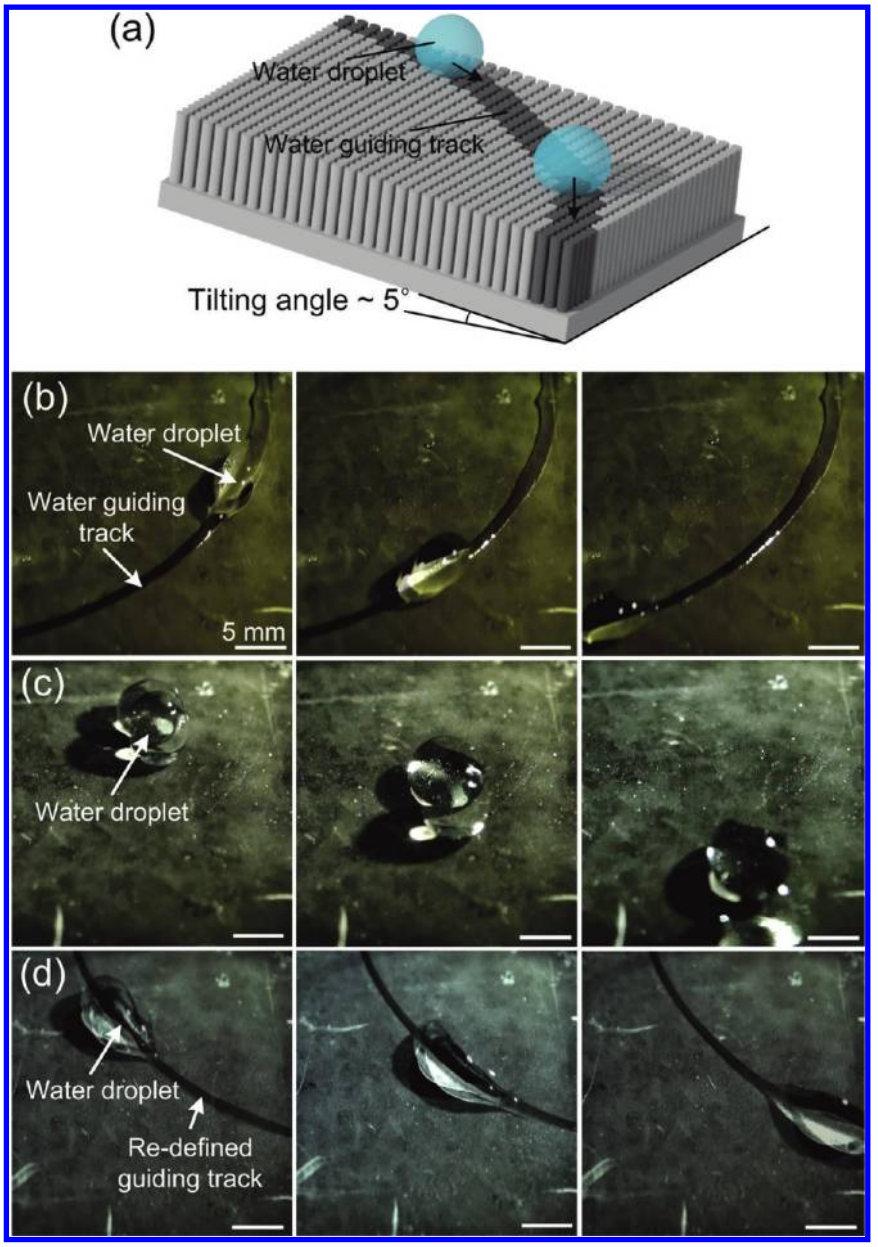

Figure 6. (a) Schematic illustration of the tilted water guiding track indicating the tilting direction of the substrate. Sequential photographs of water droplets on (b) the water guiding track, (c) re-DTS-coated surface of Si NW arrays, and (d) redefined water guiding track (right), when the substrate were tilted to 5°.

moving water droplet on a DTS modified Si NW array with a hydrophilic water guiding track. Water droplets on superhydrophobic−hydrophilic patterned Si NW arrays moved along the predefined hydrophilic pathways given a small tilt angle. Compared to the unpatterned superhydrophobic Si NW arrays, the velocity of the moving water droplet in the patterned hydrophilic water guiding track was reduced to approximately 42% of the velocity on the unpatterned substrate due to the increased interaction between the water droplet and the patterned guiding track; the measured velocity of water droplet on the unpatterned substrate was 16.54 cm/s and 6.91 cm/s on the patterned substrate. Notably, when the DTS molecules were not fully decomposed which resulted in a relatively small wettability contrasts (when t_i < 150 min), the water droplets could not be successfully transported along the curved patterned line and were stuck at defects (sites where the DTS were not fully decomposed) in the hydrophilic water guiding track during their displacement. The resulting velocity of the water droplet in the hydrophilic-superhydrophobic water guiding track is comparable to the previous research on liquid transportation using geographically patterned superhydrophobic water guiding track[6] and much faster (more than 3 times) than that in previous studies based on the surface energy gradient on a flat surface[41−44] due to the significantly reduced friction which can be attributed to the reduced contact area between the water pathway and the water droplet during the displacement. Figure 6c shows sequential photographs of water droplet motions on recoated Si NW arrays with DTS. As the hydrophilic patterns were removed, water droplets moved in straight trajectories following the gravity gradient at the same tilt angle of 5°. A new superhydrophobic−hydrophilic track with a mirror image of Figure 6b was then defined by an

additional decomposition process of UV exposure to the same sample (Figure 6d). The water droplets successfully moved along the new pathway, illustrating that the UV-patterned superhydrophobic–hydrophilic tracks could be redefined on the same substrate.

Macroscopically, the guiding process of the water droplets can be affected by two forces parallel to the substrate: the gravitation of the water droplet and the interaction force between the water droplet and the substrate. When the gravitation force is larger than that of the interaction, the water droplet begins to slide. As shown in Figure 7a, the interaction

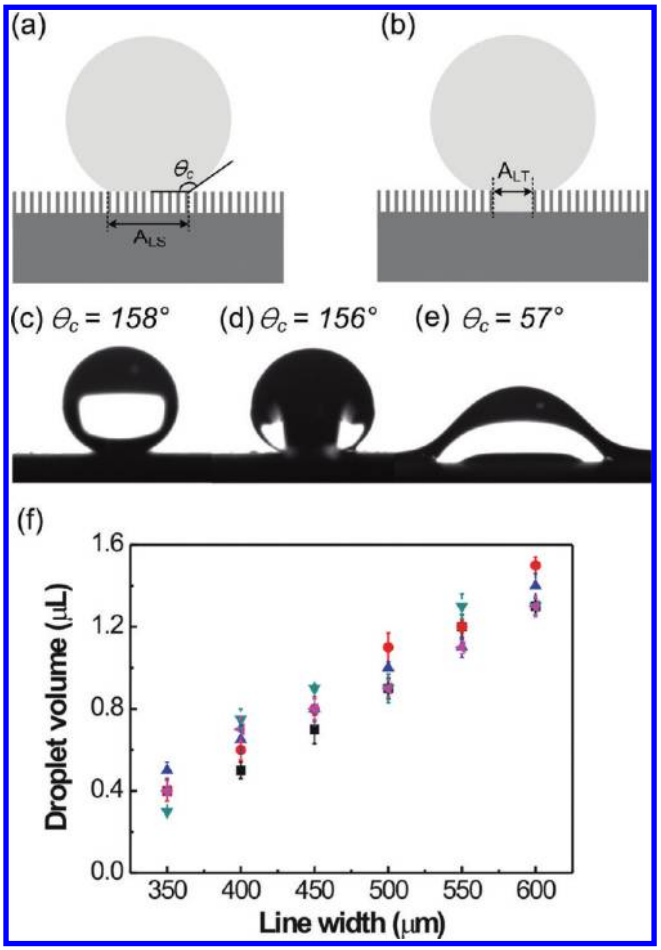

Figure 7. Schematic illustration of a water droplet on (a) DTS-coated Si NW arrays and (b) water guiding track patterned Si NW arrays. Optical images of an 8 μL water droplet on (c) DTS-coated and (c, d) water guiding track patterned Si NW arrays. The image in d was taken along the line and c was taken perpendicular to the line pattern. (f) Critical volume of the water droplets which can be transported along the water guiding track in a spherical shape with respect to the line width of the guiding tracks.

force (F_{int}) of a liquid on a surface is a function of the liquid surface tension (γ_L), static contact angle (θ_c), and the liquid–solid contact area (A_{LS}), given by the Young–Dupre equation[22,45]

$$F_{int} = \gamma_L(1 + \cos\theta_c)A_{LS} \quad (5)$$

When a liquid droplet is dropped on the hydrophilic patterned water guiding track, an additional adhesion force (F_{adh}) between the track and liquid should also be considered. Assuming a liquid-filled hydrophilic guiding track and a flat separation interface between the droplet and the liquid in the track, the overall interaction force ($F_{overall}$) of the droplet on the hydrophilic patterned substrate could be calculated as follows

$$F_{overall} = F_{int} + F_{adh} = \gamma_L(1 + \cos\theta_c)A_{LS'} + 2\gamma_L A_{LT} \quad (6)$$

where A_{LS}' is the liquid–solid interface around the track, and A_{LT} is the contact area between the hydrophilic track and the droplet (see Figure 7b). Figure 7c shows the optical photograph of an 8 μL water droplet on the DTS-coated Si NW arrays. Using 72.8 mN/m as the surface tension of water, a contact angle of 158°, and a measured contact radius of 1.5 mm, the interaction force of the water droplet on the unpatterned DTS-coated Si NW arrays can be calculated to be about 37 nN. The water CA turned to be anisotropic when a water droplet was dropped onto the hydrophilic water guiding track. Images d and e in Figure 7 present the optical photograph images of a water droplet placed on the line-patterned water guiding track; Figure 7d was taken along the line, and Figure 7e was taken perpendicular to the line. There were no significant changes in the static water CA along the line direction, whereas the water CA perpendicular to the line decreased to 57° because the water droplet was spread out along the line direction due to the capillary force. Then, the overall interaction force of an 8 μL water droplet on the hydrophilic water guiding track (line width of 500 μm) can be calculated to be 253.7 nN. The overall interaction force largely depends on the adhesion force between the track and liquid droplet, which can be adjusted by varying the line width. The capillary force could affect not only the anisotropic water CAs, but the transportation of water droplets along the hydrophilic water guiding tracks. Figure 7f exhibits the experimental results of the critical volume of water droplets (V_c) that enable water droplet transportation in a spherical shape at a certain line width of the hydrophilic water guiding track. It was observed that the water droplets spread out through the hydrophilic water guiding tracks rather than being transported with a spherical shape when the volume of the water droplets were not reached to V_c, due to the capillary force in the guiding tracks. To characterize V_c, the line width of the hydrophilic water guiding tracks were varied from 350 to 600 μm and the corresponding V_c were measured. The measured values of V_c were obtained from five different samples for each track. As shown in Figure 7f, V_c at which the droplet could be moved in a spherical shape linearly increases with the line widths of the guiding track. It may be attributed to the fact that the capillary force in the hydrophilic water guiding track is linearly increased with the line width.[46] When the volume of the dropped water droplet is larger than V_c, the droplet were transported, but it wetted the hydrophilic tracks when its volume is smaller than V_c.

In addition, several hydrophilic guiding tracks could be cross-linked and combined into a single guiding track, and transport of various aqueous solutions such as CdSe nanoparticle suspension, coffee, and rat blood was possible, as shown in Figure 8 and the video in the Supporting Information. For a comparison, the same DTS coating and selective patterning process of water guiding tracks on a flat Si substrate were carried out. Similar to the DTS-coated Si NW arrays, the water CAs on the DTS-coated flat Si substrate were gradually decreased from 109.3 to 10.1° and saturated with increasing t_i to 70 min, as shown in Figure S3 in the Supporting

dx.doi.org/10.1021/am2011756 | ACS Appl. Mater. Interfaces 2011, 3, 4722–4729

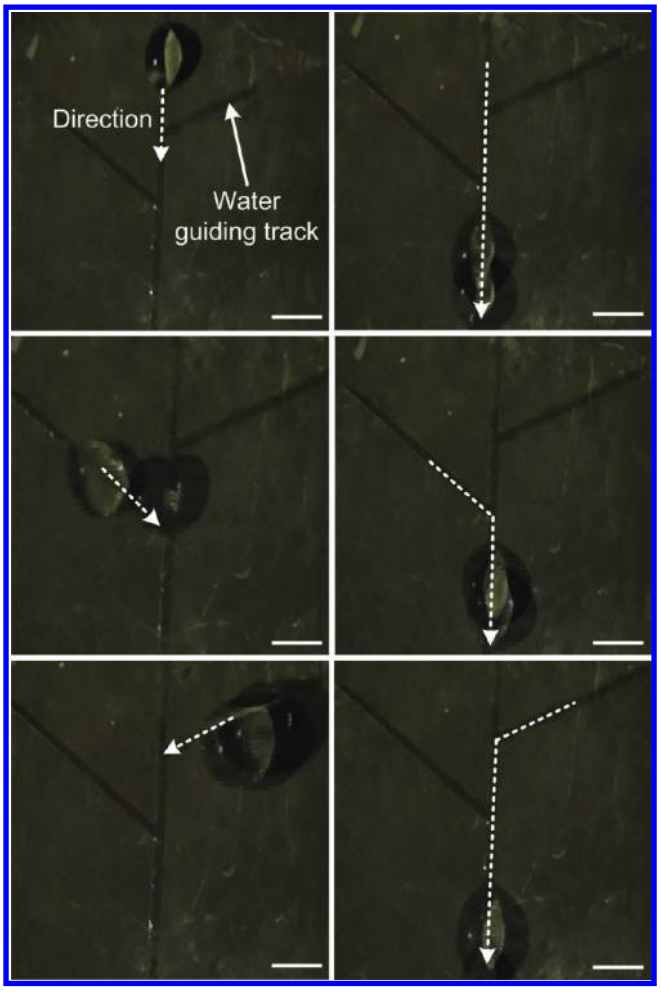

Figure 8. Sequential photographs of water droplets on cross-linked hydrophilic water guiding tracks. The scale bars in the images indicate 3 mm.

Information; the decreased photodecomposition time at a flat Si substrate compared to the Si NW substrate could be attributed to the significantly decreased surface area of the flat substrate. However, an 8 μL water droplet on the DTS-coated flat Si substrate did not roll off but stuck to the surface even at the high substrate tilting angle of 40°. In addition, water droplets could not be transported along the hydrophilic pathways. The results could be mainly ascribed to the following factors: less hydrophobicity of the DTS-coated flat Si substrate and relatively high interaction force between the substrate and water droplet.

4. CONCLUSION

In summary, we demonstrated a simple method to create hydrophilic patterns on superhydrophobic Si NW arrays to guide water droplets. Superhydrophobic Si NW arrays were obtained by coating with DTS. The superhydrophobic surfaces showed extreme water repellent properties, which can be explained by the Cassie state model. The UV-enhanced photodecomposition of DTS-coated on Si NWs allowed the wettability conversion of the surfaces of Si NW arrays from superhydrophobic to hydrophilic. A selective UV exposure process was used to produce superhydrophobic–hydrophilic patterned water guiding tracks. Water droplets on patterned Si NW arrays moved precisely along the trajectories of the hydrophilic tracks due to water surface tension, water adhesive properties of the hydrophilic patterns, and large wettability contrasts between superhydrophobic and hydrophilic regions. Furthermore, the UV-enhanced patterns on Si NW arrays could be redefined by repeating the surface modification and UV exposure process using the same substrates. We have provided a cost-effective and facile approach that can be easily integrated into conventional Si-based electronics to explore novel functions in chemical, biological, and optical applications.

■ ASSOCIATED CONTENT

Ⓢ Supporting Information

Further XPS spectral analyses of the DTS-coated Si NW arrays and a video of the moving liquid droplets on the hydrophilic patterned superhydrophobic Si NW arrays are provided in the Supporting Information. This material is available free of charge via the Internet at http://pubs.acs.org

■ AUTHOR INFORMATION

Corresponding Author

*E-mail: taeyoon.lee@yonsei.ac.kr.

■ ACKNOWLEDGMENTS

This research was supported in part by the Converging Research Center Program through the Ministry of Education, Science and Technology (2011K000631) and by the Priority Research Centers Program through the National Research Foundation of Korea (NRF) funded by the Ministry of Education, Science and Technology (2009-0093823). This work was also supported by the KARI-University Partnership program and a National Research Foundation of Korea (NRF) grant funded by the Korean government (MEST) (2011-0028594).

■ REFERENCES

(1) Zimmermann, J.; Reifler, F. A.; Fortunato, G.; Gerhardt, L.-C.; Seeger, S. *Adv. Funct. Mater.* **2008**, *18*, 3662–3669.
(2) Wang, L.; Zhang, X.; Li, B.; Sun, P.; Yang, J.; Xu, H.; Liu, Y. *ACS Appl. Mater. Interfaces* **2011**, *3*, 1277–1281.
(3) Gao, X.; Yan, X.; Yao, X.; Xu, L.; Zhang, K.; Zhang, J.; Yang, B.; Jiang, L. *Adv. Mater.* **2007**, *19*, 2213–2217.
(4) Chevallier, P.; Turgeon, S.; Sarra-Bournet, C.; Turcotte, R.; Laroche, G. *ACS Appl. Mater. Interfaces* **2011**, *3*, 750–758.
(5) Shirtcliffe, N. J.; McHale, G.; Newton, M. I.; Zhang, Y. *ACS Appl. Mater. Interfaces* **2009**, *1*, 1316–1323.
(6) Mertaniemi, H.; Jokinen, V.; Sainiemi, L.; Franssila, S.; Marmur, A.; Ikkala, O.; Ras, R. H. A. *Adv. Mater.* **2011**, *23*, 2911–2914.
(7) Shirtcliffe, N. J.; McHale, G.; Newton, M. I.; Perry, C. C.; Pyatt, F. B. *Appl. Phys. Lett.* **2006**, 89.
(8) Blossey, R. *Nat. Mater.* **2003**, *2*, 301–306.
(9) Gau, H.; Herminghaus, S.; Lenz, P.; Lipowsky, R. *Science* **1999**, *283*, 46–49.
(10) Hong, L.; Pan, T. *Microfluid. Nanofluid.* **2011**, *10*, 991–997.
(11) Parker, A. R.; Lawrence, C. R. *Nature* **2001**, *414*, 33–34.
(12) Lapierre, F.; Piret, G.; Drobecq, H.; Melnyk, O.; Coffinier, Y.; Thomy, V.; Boukherroub, R. *Lab Chip* **2011**, *11*, 1620–1628.
(13) Piret, G. l.; Desmet, R. m.; Diesis, E.; Drobecq, H.; Segers, J. r.; Rouanet, C.; Debrie, A.-S.; Boukherroub, R.; Locht, C.; Melnyk, O. *J. Proteome Res.* **2010**, *9*, 6467–6478.
(14) Piret, G. l.; Drobecq, H.; Coffinier, Y.; Melnyk, O.; Boukherroub, R. *Langmuir* **2010**, *26*, 1354–1361.
(15) Galopin, E.; Piret, G.; Szunerits, S.; Lequette, Y.; Faille, C.; Boukherroub, R. *Langmuir* **2009**, *26*, 3479–3484.
(16) Piret, G.; Galopin, E.; Coffinier, Y.; Boukherroub, R.; Legrand, D.; Slomianny, C. *Soft Matter* **2011**, *7*, 8642–8649.

(17) Leung, K. C.-F.; Xuan, S.; Lo, C.-M. *ACS Appl. Mater. Interfaces* **2009**, *1*, 2005−2012.
(18) Jokinen, V.; Sainiemi, L.; Franssila, S. *Adv. Mater.* **2008**, *20*, 3453−3456.
(19) Jonsson-Niedziolka, M.; Lapierre, F.; Coffinier, Y.; Parry, S. J.; Zoueshtiagh, F.; Foat, T.; Thomy, V.; Boukherroub, R. *Lab Chip* **2011**, *11*, 490−496.
(20) Piret, G.; Coffinier, Y.; Roux, C.; Melnyk, O.; Boukherroub, R. *Langmuir* **2008**, *24*, 1670−1672.
(21) Xu, Q. F.; Wang, J. N.; Smith, I. H.; Sanderson, K. D. *Appl. Phys. Lett.* **2008**, *93*, 233112.
(22) Mumm, F.; van Helvoort, A. T. J.; Sikorski, P. *ACS Nano* **2009**, *3*, 2647−2652.
(23) Kang, S. M.; You, I.; Cho, W. K.; Shon, H. K.; Lee, T. G.; Choi, I. S.; Karp, J. M.; Lee, H. *Angew. Chem., Int. Ed.* **2010**, *49*, 9401−9404.
(24) Zhang, X.; Jin, M.; Liu, Z.; Tryk, D. A.; Nishimoto, S.; Murakami, T.; Fujishima, A. *J. Phys. Chem. C* **2007**, *111*, 14521−14529.
(25) Rizzello, L.; Shankar, S. S.; Fragouli, D.; Athanassiou, A.; Cingolani, R.; Pompa, P. P. *Langmuir* **2009**, *25*, 6019−6023.
(26) Stojanovic, A.; Artus, G. R. J.; Seeger, S. *Nano Res.* **2010**, *3*, 889−894.
(27) Garrod, R. P.; Harris, L. G.; Schofield, W. C. E.; McGettrick, J.; Ward, L. J.; Teare, D. O. H.; Badyal, J. P. S. *Langmuir* **2007**, *23*, 689−693.
(28) Zhu, X.; Zhang, Z.; Men, X.; Yang, J.; Xu, X. *ACS Appl. Mater. Interfaces* **2010**, *2*, 3636−3641.
(29) Peng, K.; Fang, H.; Hu, J.; Wu, Y.; Zhu, J.; Yan, Y.; Lee, S. *Chem.—Eur. J.* **2006**, *12*, 7942−7947.
(30) Chen, C. Y.; Wu, C. S.; Chou, C. J.; Yen, T. J. In *Adv. Mater.* **2008**; Vol. *20*; pp 3811-3815.
(31) Wei-Fan, K.; Li-Jen, C. *Nanotechnology* **2009**, *20*, 035605.
(32) Kim, B. S.; Shin, S.; Shin, S. J.; Kim, K. M.; Cho, H. H. *Langmuir* **2011**, *27*, 10148−10156.
(33) Cassie, A. B. D.; Baxter, S. *Trans. Faraday Soc.* **1944**, *40*, 546−551.
(34) Peng, K.; Huang, Z.; Zhu, J. *Adv. Mater.* **2004**, *16*, 73−76.
(35) Bhattacharya, P.; Gohil, S.; Mazher, J.; Ghosh, S.; Ayyub, P. *Nanotechnology* **2008**, *19*, 075709.
(36) Ye, T.; Wynn, D.; Dudek, R.; Borguet, E. *Langmuir* **2001**, *17*, 4497−4500.
(37) Kwak, G.; Lee, M.; Senthil, K.; Yong, K. *Langmuir* **2010**, *26*, 12273−12277.
(38) Frydman, E.; Cohen, H.; Maoz, R.; Sagiv, J. *Langmuir* **1997**, *13*, 5089−5106.
(39) Wang, S. J.; Lim, P. C.; Huan, A. C. H.; Liu, C. L..; Chai, J. W.; Chow, S. Y.; Pan, J. S.; Li, Q.; Ong, C. K. *Appl. Phys. Lett.* **2003**, *82*, 2047−2049.
(40) Tamura, T.; Adachi, S. *J. Appl. Phys.* **2009**, *105*, 113518.
(41) Chaudhury, M. K.; Whitesides, G. M. *Science* **1992**, *256*, 1539−1541.
(42) Bain, C. D.; Burnett-Hall, G. D.; Montgomerie, R. R. *Nature* **1994**, *372*, 414−415.
(43) Gallardo, B. S.; Gupta, V. K.; Eagerton, F. D.; Jong, L. I.; Craig, V. S.; Shah, R. R.; Abbott, N. L. *Science* **1999**, *283*, 57−60.
(44) Lee, S.-W.; Laibinis, P. E. *J. Am. Chem. Soc.* **2000**, *122*, 5395−5396.
(45) Bangham, D. H.; Razouk, R. I. *Trans. Faraday. Soc.* **1937**, *33*, 1459−1463.
(46) Yang, D.; Krasowska, M.; Priest, C.; Popescu, M. N.; Ralston, J. *J. Phys. Chem. C* **2011**, *115*, 18761−18769.